in pulmonary atresia with intact ventricular septum. *Pediatrics* 2006 ; 118 : e415-420
17) Jaeggi ET, Fouron JC, Silverman ED, et al : Transplacental fetal treatment improves the outcome of prenatally diagnosed complete atrioventricular block without structural heart disease. *Circulation* 2004 ; 110 : 1542-1548
18) Schmidt KG, Ulmer HE, Silverman NH, et al : Perinatal outcome of fetal complete atrioventricular block : a multicenter experience. *J Am Coll Cardiol* 1991 ; 17 : 1360-1366
19) Carpenter RJ Jr, Strasburger JF, Garson A Jr, et al : Fetal ventricular pacing for hydrops secondary to complete atrioventricular block. *J Am Coll Cardiol* 1986 ; 8 : 1434-1436
20) Walkinshaw SA, Welch CR, McCormack J, Walsh K : In utero pacing for fetal congenital heart block. *Fetal Diagn Ther* 1994 ; 9 : 183-185
21) Kikuchi Y, Shiraishi H, Igarashi H, et al : Cardiac pacing in fetal lambs: intrauterine transvenous cardiac pacing for fetal complete heart block. *Pacing Clin Electrophysiol* 1995 ; 18 : 417-423
22) Pavlovic M, Acharya G, Huhta JC : Controversies of fetal cardiac intervention. *Early Hum Dev* 2008 ; 84 : 149-153

O-029 Canceled

O-030 Pulmonary Vessel Occlusion Using High-intensity Focused Ultrasound (HIFU): Is It Useful for Minimally Invasive Treatment of Fetal Chest Mass?

Noriyoshi Nakayama[1], Akihiko Ishiyama[1], Tetsuko Ishii[1], Hiromasa Yamashita[1], Yoshitaka Miyamoto[1], Toshinobu Miyoshi[1], Takashi Azuma[3], Toshio Chiba[1], Akira Toki[2]

(National Center for Child Health and Development, Japan[1], Department of Pediatric Surgery, Showa University[2], Central Research Laboratory, Hitachi Ltd[3])

Background: To reduce the size of life-threatening fetal chest mass, ultrasound-guided cyst decompression or open fetal lobectomy has been employed depending on its morphology. However, these technically demanding procedures are still invasive and are unsatisfactory in terms of their clinical outcome. We present the result of our experiments to achieve much less invasive mass reduction by thermal coagulation of the feeding vessels using high-intensity focused ultrasound (HIFU). Materials and Methods: Japanese white rabbits (male, 2.8kg) were anesthetized and intubated for mechanical ventilation, and underwent thoracotomy for placing an unilateral bronchial blocker for differential ventilation. The entire distal airway of the occluded lung was completely filled with degassed saline to produce a fluid-filled fetal lung model which has sonographically visualized intrapulmonary vessels. Using color Doppler sonography, the target pulmonary vessel to be occluded was located and treated with a total of three HIFU irradiations (3.3MHz; 10sec. each with an interval of 30sec.). Results: By HIFU irradiation, we could successfully cease the targeted blood flow. Pathological examinations revealed thermally coagulated vessels. Conclusion: HIFU was feasible for vessel occlusion in vivo using experimentally fluid-filled animal lungs. HIFU irradiation might be useful for quicker and safer reduction of a fetal chest mass.

Computer-Aided Delivery of High-Intensity Focused Ultrasound (HIFU) for Creation of an Atrial Septal Defect in Vivo

Hiromasa Yamashita[1], Tetsuko Ishii[1], Akihiko Ishiyama[1], Noriyoshi Nakayama[1], Toshinobu Miyoshi[1], Yoshitaka Miyamoto[1], Gontaro Kitazumi[1], Yasumasa Katsuike[1], Makoto Okazaki[2], Takashi Azuma[3], Masayuki Fujisaki[4], Shinichi Takamoto[4], and Toshio Chiba[1]

[1] Department of Strategic Medicine, National Center for Child Health and Development. 2-10-1, Okura, Setagaya-ku, Tokyo, Japan
{yamashita-h, ishii-t, ishiyama-a, nakayama-n, chiba-t, kitazumi-g, katsuike-y}@ncchd.go.jp, {tmiyoshi, ymiyamoto}@nch.go.jp
http://www.ncchd.go.jp/

[2] Infinity Medicalsoft Co.,Ltd. 2120-6-102, Higashi-naganuma, Inagi-shi, Tokyo, Japan
mokazaki@inf-medicalsoft.co.jp
http://www.inf-medicalsoft.co.jp/

[3] Central Resarch Laboratory, Hitachi Ltd. 1-280, Higashi-koigakubo, Kokubunji-shi, Tokyo, Japan
takashi.azuma.sa@hitachi.com
http://www.hqrd.hitachi.co.jp/crl/index.cfm

[4] Department of Cardiothoracic Surgery, Graduate School of Medicine, University of Tokyo. 7-3-1, Hongo, Bunkyo-ku, Tokyo, Japan
masafujicardio@yahoo.co.jp, takamoto-tho@h.u-tokyo.ac.jp
http://ctstokyo.umin.ne.jp/

Abstract. In recent years, several fetal cardiac malformations have been increasingly treated before birth with gradually improved outcome, although the technique is still demanding and invasive. We newly developed a computer-aided system for energy delivery of high-intensity focused ultrasound (HIFU) to correct cardiac morphologic abnormalities *in vivo* much less invasively. The HIFU system could be controlled in real-time by a computer-based analysis of 2D-sonographic left ventricular images for optimal triggering off HIFU. Using beating heart of two anesthetized adult rabbits, the system successfully achieved a non-touch gross ablation of the atrial septum in one animal, and in the other HIFU energy was inadvertently mistargeted on the posterior wall of the left atrium with a resultant small transmural opening. We believe that the HIFU system will be introduced with pinpoint accuracy to minimally invasive treatment of fetal cardiac abnormalities that have intact or highly restrictive atrial septum.

Keywords: Fetal cardiac intervention, Computer-aided HIFU energy delivery, Real-time sonographic image analysis.

1 Introduction

Several fetal cardiac malformations have been increasingly treated before birth. Fetal cardiac intervention targets an in utero correction of simple intracardiac abnormalities

T. Dohi, I. Sakuma, and H. Liao (Eds.): MIAR 2008, LNCS 5128, pp. 300–310, 2008.

that potentially progress to complex heart diseases in utero, such as fetal critical aortic stenosis that might advance to hypoplastic left heart syndrome (HLHS) and HLHS with restrictive atrial septum leading to irreversible pulmonary vascular damages ([1]-[3]). Current fetal procedures for correction of restrictive atrial septum with an atrial decompression are still invasive because they, percutaneously and through both the uterine and fetal chest walls, require ultrasound-guided maternal puncture into the pulsating cardiac cavity of tiny fetal hearts and to create interatrial communications. Accordingly, these procedures have been reportedly accompanied by serious complications including profound bradycardia, bleeding and hemopericardium, intracardiac thrombus formation, and recurrent in utero closure of the created atrial septal defects.

Instead, to accomplish our goal of establishing fetal interatrial communications with minimal adverse effects, we developed an entirely new approach with the use of high-intensity focused ultrasound (HIFU). HIFU is an acoustic modality using ultrasound energy (cavitation or coagulation or both) focused to operate on an internally targeted tissue without damaging overlying and/or underlying tissues. Accordingly, HIFU has been employed predominantly for non-touch treatment of tumors including prostate cancer and uterine fibroids ([4], [5]). Unlike an extensive ablation of stationary tumors, the HIFU ablation to a pulsating narrow area in the beating and tiny fetal heart requires a pinpoint accuracy based on computer-aided target autotracking capacity. We originated a precise HIFU delivery device coupled with a real-time computer-aided 2D ultrasound image analysis. In this article, we report the outcome of our feasibility study for atrial septal defect creation using the beating heart of anesthetized adult rabbits.

2 Material and Methods

2.1 System Configuration

The system configuration of the computer-aided HIFU energy delivery system consists of predominantly 4 parts (Fig. 1). The first one is a HIFU energy delivery device which comprises a monocoque spherical shaped piezo transducer (PZT) and a diagnostic 2D-US imaging probe. The tomographic images of the latter include the focal point of the former. Radius of the PZT curvature is 40 mm, and the focal point is elliptical in shape (0.6-mm wide, 5.0-mm long). Focal point is located 40-mm apart from the PZT edge face. The second part is a diagnostic 2D-US imaging equipment (EnVisor C HD, Philips, Andover, MA) to drive a 2D-US imaging probe (s12, Philips, Andover, MA) and to do sector scanning of a cardiac four-chamber view. The equipment outputs grayscale NTSC-video data (640x480 pixels) into the workstation with 30 frames/sec. The third part is a signal generator (Agilent 33220A, Agilent technologies, Santa Clara, CA) and RF power amplifier (AG1012, T&C power Conversion Inc., Rochester, NY) to drive the PZT with a 3.3-MHz sine-wave. Input voltage into the PZT is about 160 Vpp from and temporal average intensity of the continuous-wave spatial peak is 6.5 kW/cm^2. The fourth part is a workstation (HP xw8200, OS:WindowsXP Pro SP2, CPU:Intel Xeon 3.8 GHz, Memory:2 GB, GPU:NVIDIA Quadro FX3450) to analyze input 2D-US tomographic image of cardiac four-chamber with our original real-time HIFU energy delivery control algorithm. A capture board (MTPCI-DC2,

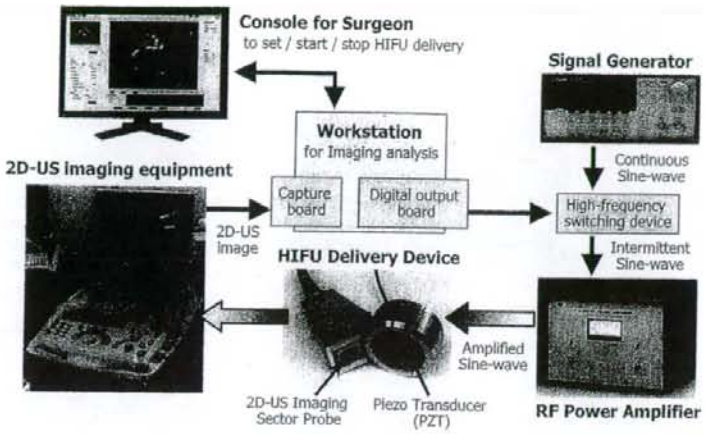

Fig. 1. System configuration of the computer-aided HIFU energy delivery

MICRO-TECHNICA, Tokyo, Japan) rasterizes the 2D-US image with an image-processing sub-system (Image-Pro. Plus. MediaCybernetics, Inc., Bethesda, MD) to analyze a cardiac beating cycle of the target. According to the analysis outcome, a digital I/O board (PIO-16/16L(LPCI)H, Contec CO., Ltd., Osaka, Japan) outputs the trigger signals for HIFU energy delivery into the high-frequency switching device to switch HIFU energy delivery ON/OFF.

2.2 Control of HIFU Energy Delivery

We developed an algorithm to recognize a cardiac beating cycle and to control a computer-aided HIFU energy delivery to an atrial septum based on prediction of its proper timing. Although cardiac beating motion is spatial, the atrial septum is not so moved spatially in the beating heart but contracted and stretched in sync with the cardiac beating motion. So with 2D-US tomographic image including the atrial septum, our system decides HIFU energy delivery timing. This software works with the following sequence.

1. Setting the position of HIFU energy delivery device
2. Accumulating cardiac beating cycle to recognize the optimal timing of HIFU energy delivery by 2D-US tomographic image
3. Computer-aided HIFU energy delivery to the atrial septum
4. Confirmation of an interatrial communication by color Doppler US
5. Repeat HIFU energy delivery to achieve an interatrial communication

Initial setting of the HIFU energy delivery system. Firstly, an operator positions the HIFU energy delivery device to scan the four-chamber view sighting the PZT focal point on the atrial septum. The HIFU energy beam should be directed perpendicular to the atrial septum as much as possible. Resolution for image analysis of the captured

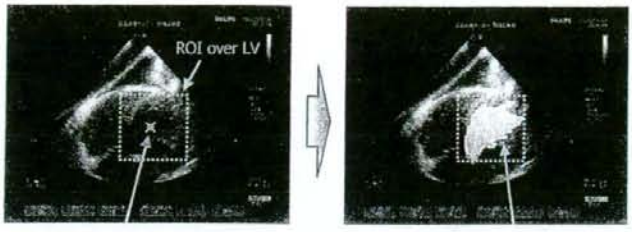

Fig. 2. Region of interest is set by the operator to extract a polygonal area of the left ventricle in the captured 2D-US four-chamber view

2D-US sector view is 0.2 mm in the beam direction which depends on display resolution, and 0.5-mm in the angular orientation which depends on sector angle and depth of region of interest (ROI).

Secondly, the operator sets a suitable rectangle ROI surrounding the left ventricle (LV) on the 2D-US images and indicates a single position within the LV. The system binarizes and extracts the polygonal area of LV (total number of pixels) (Fig. 2). In the animal experiments, the LV area includes the target's high-frequency cardiac beating (CB) element and low-frequency respiration element. The latter is controlled to be 20 cycles/min by an artificial respiration (AR). In order to separate the AR element from the CB element, we use a running average of the LV area for a low-pass filter with a small calculation amount. Where the time is t, the LV area is $S_{LV}(t)$ and the AR element is $S_{AR}(t)$, $S_{AR}(t)$ is shown in the equation (1) with sampling time Δt and a running average of $S_{LV}(t)$. N is sampling number to get the running average. According to Fourier transformation, when the running average is with sampling number six, only the AR element can be extracted from the LV area.

$$S_{AR}(t) = \frac{1}{N}\sum_{n=0}^{N-1} S_{LV}(t - n\Delta t) \tag{1}$$

Accordingly the CB element $S_{CB}(t)$ is shown in the equation (2) without high-frequency noise (more than 15 Hz) by averaging a current value $S_{LV}(t)$ and an adjacent value $S_{LV}(t - \Delta t)$ (Fig. 3).

$$S_{CB}(t) = \frac{S_{LV}(t) + S_{LV}(t - \Delta t)}{2} - S_{AR}(t) \tag{2}$$

Furthermore, with the calculation of an average cardiac beating cycle T_{CB}, maximum and minimum values of $S_{CB}(t)$ (MAX_{CB} and MIN_{CB}) and of $S_{AR}(t)$ (MAX_{AR} and MIN_{AR}) can be registered automatically.

Timing determination of HIFU energy delivery. Duration of each HIFU energy delivery is set 1/3 of the average time of cardiac beating cycle and the delivery should

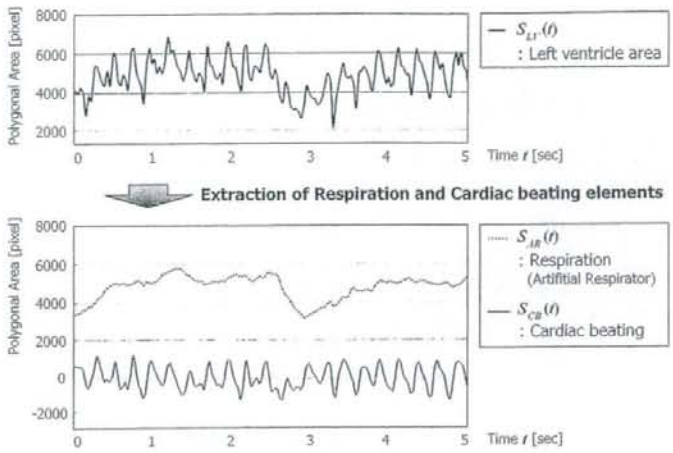

Fig. 3. Extraction of the respiration element ($S_{AR}(t)$) and the cardiac beating element ($S_{CB}(t)$) from the left ventricle polygonal area ($S_{LV}(t)$)

be triggered off from the moment when $S_{CB}(t)$ becomes a local minimal value in systolic period, or when the atrial septum is most stretched. The HIFU energy delivery is performed in real time (more than 25 frames/sec), although there is a certain time delay (total 69 ms) in the sequence of 2D-US image input (30 ms), rasterizing and image analysis (30 ms), and HIFU energy delivery signal output (9 ms). Therefore, the system needs a predictive control to cancel this time delay, which is shown by D. To estimate the HIFU energy delivery timing, which is shown by t_P, the system uses the moment t_M when $S_{CB}(t)$ achieves around the local maximal value. To determine the moment t_M, with a sampling interval of Δt, a current value $S_{CB}(t)$ and a difference value $\Delta S_{CB}(t)$ between $S_{CB}(t)$ and $S_{CB}(t-\Delta t)$ are used (Fig. 4). Next, t_P is estimated as $t_M + T_{CB}/2$ and HIFU energy delivery can be triggered from the moment $t_P - D$.

Furthermore, to avoid inadvertent HIFU deliveries caused by abnormal cardiac rhythms, unexpected target behavior, false recognitions in imaging analysis and so on, the HIFU energy delivery timing is constrained strictly by two boundary conditions with the tolerance range T_{CB} for $S_{CB}(t)$ and the tolerance range T_{AR} for $S_{AR}(t)$ (Fig. 5). In this study, T_{CB} is set $(MAX_{CB} - MIN_{CB}) \times 20\%$, and T_{AR} is set $(MAX_{AR} - MIN_{AR}) \times 30\%$.

3 Animal Experiments

All animal experiments were performed according to the institutional animal ethics guidelines, based on the guidelines of the National Institute of Health, USA[7].

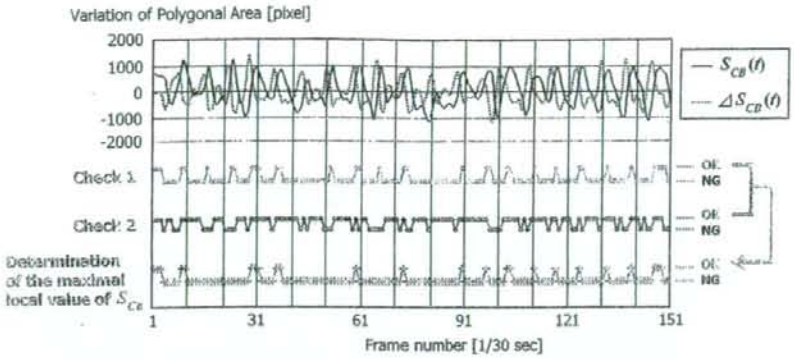

Fig. 4. Determination whether $S_{CB}(t)$ achieves around local maximal value or not. If $S_{CB}(t)$ comes close to MAX_{CB} enough (for example $S_{CB}(t) > MAX_{CB} \times 50\%$) (Check 1 is "OK") and if $\Delta S_{CB}(t)$ comes to 0 enough (for example $\mid \Delta S_{CB}(t) \mid < (MAX_{CB} - MIN_{CB}) \times 30\%$) (Check 2 is "OK"), that moment t is determined t_M.

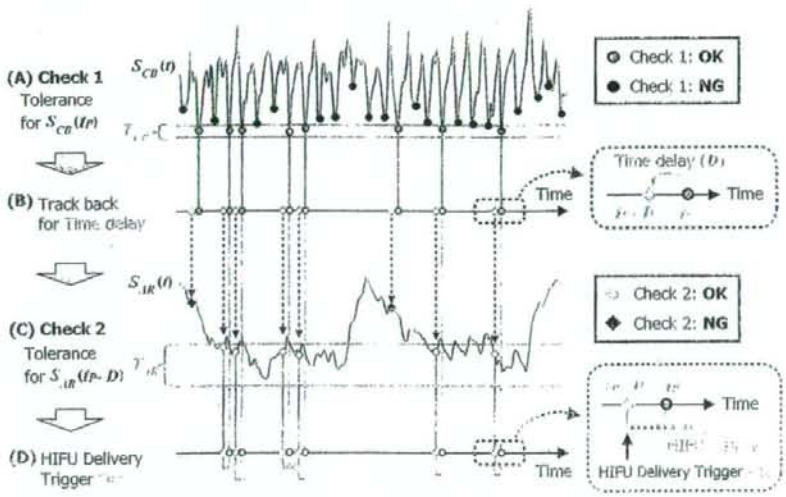

Fig. 5. Prevention of inadvertent HIFU energy delivery by means of two boundary conditions. (A) Check 1 for $S_{CB}(t_P)$: Whether $S_{CB}(t_P)$ falls in the tolerance range T_{CB} or not, that is $MIN_{CB} \leq S_{CB}(t_P) \leq MIN_{CB} + T_{CB}$. (B) If Check 1 is cleared, the moment $t_P - D$ is considered. (C) Check 2 for $S_{AR}(t_P - D)$: Whether $S_{AR}(t_P - D)$ falls in the tolerance range T_{AR} or not, that is $MIN_{AR} \leq S_{AR}(t_P - D) \leq MIN_{AR} + T_{AR}$. (D) If Check 2 is cleared, the HIFU energy delivery is triggered at the moment of $t_P - D$.

3.1 Experimental Protocol

Two adult rabbits (Japanese White, 2.8 kg, male) were anesthetized first with lazine (5 mg/kg IM) and isoflurane inhalation. Then, after endotracheal intubatic tracheostomy placement, anesthesia was maintained on mechanical ventilation isoflurane and oxygen inhalation (20 cycles/min, 240 ml/cycle). Intraoperatively, I arterial blood pressure/oxygen saturation, and end-tidal carbon dioxide concentr were monitored in real time. The animals underwent median sternotomy to expos heart and, on both sides, chest cavities were filled with buffering gel. The beating was set in direct contact with a silicone sheet-bottomed tank filled with degassed ((37°C) (Fig. 6). A HIFU transducer combined with a diagnostic 2D-US probe fixed on a two-directional (x-y) linear stage with a pivot hinge placed in the tank v was manually steered so that the HIFU focal point could be roughly located o atrial septum of the beating heart. In advance, this focal point was properly adjust simulated polymer-coated rubber irradiation using the same system (Acoustic star Eastek Corporation, Tokyo, Japan). Fig. 7 shows the coagulated ellipsoid focal poi mm long, 2-mm wide) along with its focal length of 30-mm. Both could be visu on the 2D-US images and marked in the console. HIFU energy delivery time amo to 3,000 ms in a total for each target. As adult rabbits occasionally have a rem fetal interatrial communication, blood flows across the atrial septum may be obs on color Doppler US images prior to HIFU irradiation. Accordingly, we must the number or width of the blood flow through the atrial septum after HIFU del With pentobarbital given IV, the animals were sacrificed and, the hearts were e for pathological examination (macroscopic, microscopic). The tissue specimens

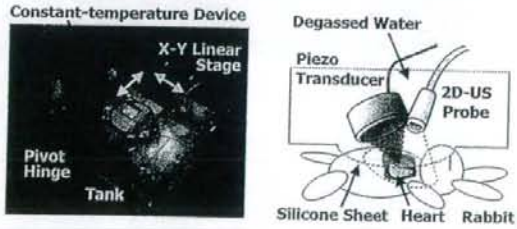

Fig. 6. Experimental setup using an adult rabbit through a water tank

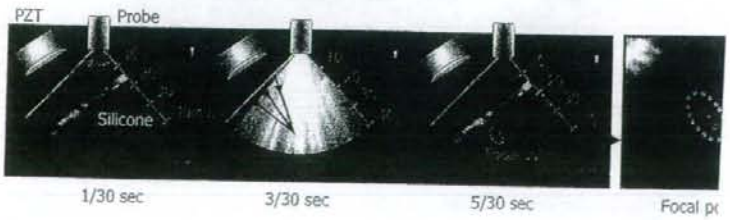

Fig. 7. The focal point is adjusted with a test HIFU energy delivery to the polymer-coate

fixed with 10% neutral formalin and embedded in paraffin. Thereafter, sections of 10 μm thickness were stained with hematoxylin-eosin (HE) for microscopic studies.

3.2 Results

In the first animal, HIFU was delivered in a total of 26 times with each delivery time of 115 ms over a total of 23 seconds for treatment. Due to an inadvertent mistargeting, the atrial septum failed to be ablated and, instead, a small opening was made in the posterior wall of the left atrium with a blood flow through there was visualized with color Doppler US during the experiment. Fig. 8 shows the gross appearance of the ablated portion. Based on the microscopic study (B) of the stained section (C), we confirmed that a small area was definitely coagulated with a resultant small transmural opening. The opening was located just behind the atrial septum along the assumed axial direction of the HIFU beam and its focal point. In the second animal experiment, 23 HIFU deliveries were carried out for a total of 57 seconds with each delivery time of 130 ms. Although the pulsating atrial septum could be autotracked and targeted precisely by our system, the atrial septum apparently remained non-penetrated with mere transmural

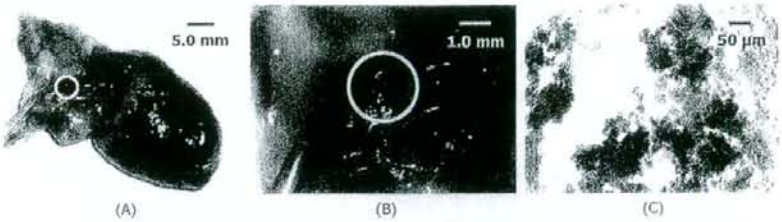

Fig. 8. Heart specimen ablated with HIFU (first animal). (A) Gross appearance of the inadvertent ablation with an opening. (B) Magnification of the area opened by HIFU irradiation. Both pictures (A, B) represent the opening of the left atrial posterior wall. (C) Microscopic findings of the ablated area (H-E stain). Coagulation changes are seen unlike the surrounding normal area.

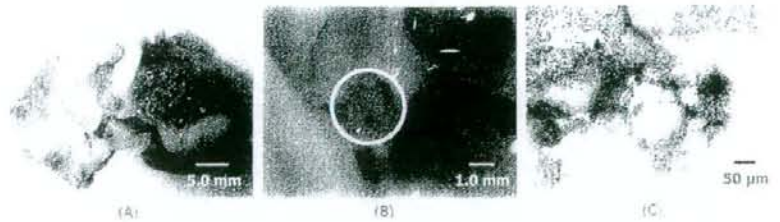

Fig. 9. Heart specimen ablated with HIFU (second animal). (A) Gross appearance of the inadvertent ablation with an opening. (B) Magnification of the area opened by HIFU irradiation. Both pictures (A, B) represent just transmural coagulation changes of the targeted atrial septum. (C) Microscopic findings of the ablated area (H-E stain). Coagulation changes are clearly found.

coagulation changes on gross appearance. It is suggested that the HIFU energy transfer was somehow reduced because it took longer to finish HIFU delivery than in the first one. When interval time of each HIFU delivery was too long, heated tissue at the focal point might be cooled down by intracardiac blood flow. Macroscopic view of the excised tissue is shown in Fig. 9. Assumingly, improvements in HIFU delivery parameters will settle the problems because a precise autotargeting was successfully achieved in our study.

4 Discussion

In this report, we demonstrated that our computer-aided HIFU delivery system, coupled with a newly developed real-time image-recognition algorithm, could create defects in the pulsating tissues of within beating hearts of anesthetized adult rabbits. Furthermore, the procedure could be expected to affect just a restricted targeted area without impairing adjacent tissues. Then, we believe that the computer-aided HIFU delivery system will contribute to developing minimally invasive correction of intracardiac abnormalities including those of fetal and pediatric patients.

In recent years, HIFU has been explored as a therapeutic modality in urology, oncology, and prostatic/breast cancer or uterine fibroids[4]-[6]. In the field of cardiology, HIFU was investigated as a promising device to treat arrhythmia, to release valvular stenosis and to ameliorate obstructive hypertrophic cardiomyopathy. HIFU also enables us to create defects in cardiac tissues such as ventricles or cusp of the aortic valve *in vitro* or *ex vivo*[8]-[13]. Worthy of note, fetal cardiac intervention has been shown to potentially prevent simple fetal cardiac abnormalities from in utero progression to serious heart diseases, although the procedure still remains an invasive technique for both the mother and fetus[1]. Then, one of our important hypotheses is that a HIFU delivery system, combined with an image-recognition algorithm, might be useful to achieve a safer, faster, and less expensive fetal procedure.

We conducted our HIFU experiment to affect intracardiac structures *in vivo* using two adult rabbits and their microscopic examination showed that all areas irradiated with HIFU presented with restricted coagulation changes with or without making a transmural opening. Our results of the experiment are not yet satisfactory in terms of accuracy of targeting and/or timing of HIFU energy delivery. In these animal models, the heart might have been malpositioned (or rotated) which resulted in non-perpendicular HIFU irradiation to the atrial septum or the HIFU focal point inadvertently set at the atrial free wall. Accordingly, we believe that creation of atrial septal defects could be accomplished more precisely with careful device/animal positioning and adjusting the direction of HIFU delivery more appropriately. For this purpose, we developed the image-recognition algorithm/software based on real-time 2D sonographic cardiac images, although the estimation of optimally timed HIFU irradiation is not yet accurate enough and has to be further improved. Moreover, to optimize the configuration (size, volume and position) of ablated lesions, we still have to identify more appropriate HIFU delivery parameters including HIFU frequency, focal depth, ratio between aperture size and focal depth, size or shape of focal point, and duration of HIFU irradiation[12]. In fact, Zhen et al. suggested that the ablation should be better performed by pulsed ultrasound. Strickberger et al. reported that ECG-triggered HIFU delivery could effectively

treat experimental arrhythmia[13]. In addition about accurate positioning of the focal point, Koizumi et al. presented HIFU irradiation with a pair of 2D-US imaging probes and XYZ positioning mechanism for 3D-tracking system[14].

In our experiment, another prospective biological limitation is that the experimental animals had normal hearts. In pathological conditions with intracardiac abnormalities, the cardiac structure including the atrial septum is occasionally hypertrophied. Accordingly, before employing the HIFU for clinical intervention, it is necessary to test the effects of HIFU using pathologic animal models.

In conclusion, the HIFU irradiation, combined with newly developed computer-aided algorithm/software, is expected to be feasible for correcting intracardiac abnormalities in beating hearts. This outcome suggests that even the current fetal cardiac intervention is likely to further advance to much less invasive one employing an integrated and sophisticated HIFU system.

Acknowledgments. A part of this work is supported by Grant Program for Child Health and Development "Minimally Invasive Techniques for Fetal Surgery (16-3)" administrated by Ministry of Health, Labour and Welfare of Japan.

References

1. Kohl, T., Sharland, G., Allan, L.D., Gembruch, U., Chaoui, R., Lopes, L.M., Zielinsky, P., Huhta, J., Silverman, N.H.: World experience of percutaneous ultrasound-guided balloon valvuloplasty in human fetuses with severe aortic valve obstruction. Am. J. Cardiol. 85, 1230–1233 (2000)
2. Marshall, A.C., van der Velde, M.E., Tworetzky, W., Gomez, C.A., Wilkins-Haung, L., Benson, C.B., Jennings, R.W., Lock, J.E.: Creation of an atrial septal defect in utero for fetuses with hypoplastic left heart syndrome and intact or highly restrictive atrial septum. Circulation 110, 253–258 (2004)
3. Makikallio, K., McElhinney, D.B., Levine, J.C., Marx, G.R., Colan, S.D., Marshall, A.C., Lock, J.E., Marcus, E.N., Tworetzky, W.: Fetal Aortic valve stenosis and the evolution of hypoplastic left heart syndrome patient selection for fetal intervention. Circulation 113, 1401–1405 (2006)
4. Rebillard, X., Gelet, A., Davin, J.L., Soulie, M., Prapotnich, D., Cathelineau, X., Rozet, F., Vallancien, G.: Transrectal high-intensity focused ultrasound in the treatment of localized prostate cancer. J. Endourol. 19(6), 693–701 (2005)
5. Chan, A.H., Fujimoto, V.Y., Moore, D.E., Martin, R.W., Vaezy, S.: An image-guided high intensity focused ultrasound device for uterine fibroids treatment. Med. Phys. 29(11), 2611 (2002)
6. Hengst, S.A., Ehrenstein, T., Herzog, H., Beck, A., Urz-Billing, I., David, M., Felix, F., Ricke, J.: Magnetic resonance tomography guided focused ultrasound surgery (MRgFUS) in tumor therapy?anew noninvasive therapy option. Radiologe 44(4), 339–346 (2004)
7. U.S. Department of Health and Human Services. Public Health Service. National Institutes of Health. Guide for the care and use of laboratory animals, pp. 85-23. NIH Publication (1985)
8. Otsuka, R., Fujikura, K., Hirata, K., Pulerwitz, T., Oe, Y., Suzuki, T., Sciacca, R., Marboe, C., Wang, J., Burkhoff, D., Muraiore, R., Lizzi, F.L., Homma, S.: In vitro ablation of cardiac valves using high-intensity focused ultrasound. Ultrasound in Med. & Biol. 31(1), 109–114 (2005)

9. Fujikura, K., Otsuka, R., Kalisz, A., Ketterling, J.A., Jin, Z., Sciacca, R.R., Marboe, C.C., Wang, J., Muratore, R., Feleppa, E.J., Homma, S.: Effects of ultrasonic exposure parameters on myocardial lesions induced by high-intensity focused ultrasound. J. Ultrasound Med. 25, 1375–1386 (2006)
10. Lee, L.A., Simon, C., Bove, L.E., Mosca, R.S., Ebbini, E.S., Abrams, G.D., Ludomirsky, A.: High intensity focused ultrasound effect on cardiac tissues: Potential for Clinical application. Echocardiography 17(6), 563–566 (2000)
11. Xu, Z., Ludmirsky, A., Eun, L.Y., Hall, T.L., Tran, B.C., Fowlkes, J.B., Cain, C.A.: Controlled ultrasound tissue erosion. IEEE transactions on ultrasonics, ferroelectrics, and frequency control 51(6), 726–736 (2004)
12. Kluiwstra, J.U.A., Tokano, T., Davis, J., Strickberger, S.A., Cain, C.A.: Real time image guided high intensity focused ultrasound for myocardial ablation: In Vivo study. In: IEEE Ultrasonics Symposium, vol. 1327 (2007)
13. Strickberger, S.A., Tokano, T., Kluiwstra, J.U.A., Morady, F., Cain, C.: Extracardiac ablation of the canine atrioventricular junction by use of high-intensity focused ultrasound. Circulation 100, 203–208 (1999)
14. Koizumi, N., Ota, K., Lee, D., Yoshizawa, S., Ito, A., Kaneko, Y., Yoshinaka, K., Matsumoto, Y., Mitsuishi, M.: Feed-forward controller for the integrated non-invasive ultrasound diagnosis and treatment. J. Robotics and Mechatronics 20(1), 89–97 (2008)

Vol 454|17 July 2008|doi:10.1038/nature07027

nature

LETTERS

IGFBP-4 is an inhibitor of canonical Wnt signalling required for cardiogenesis

Weidong Zhu[1]*, Ichiro Shiojima[1]*, Yuzuru Ito[2]*, Zhi Li[1], Hiroyuki Ikeda[1], Masashi Yoshida[1], Atsuhiko T. Naito[1], Jun-ichiro Nishi[1], Hiroo Ueno[3], Akihiro Umezawa[4], Tohru Minamino[1], Toshio Nagai[1], Akira Kikuchi[5], Makoto Asashima[2,6,7] & Issei Komuro[1]

Insulin-like growth-factor-binding proteins (IGFBPs) bind to and modulate the actions of insulin-like growth factors (IGFs)[1]. Although some of the actions of IGFBPs have been reported to be independent of IGFs, the precise mechanisms of IGF-independent actions of IGFBPs are largely unknown[1,2]. Here we report a previously unknown function for IGFBP-4 as a cardiogenic growth factor. IGFBP-4 enhanced cardiomyocyte differentiation *in vitro*, and knockdown of *Igfbp4* attenuated cardiomyogenesis both *in vitro* and *in vivo*. The cardiogenic effect of IGFBP-4 was independent of its IGF-binding activity but was mediated by the inhibitory effect on canonical Wnt signalling. IGFBP-4 physically interacted with a Wnt receptor, Frizzled 8 (Frz8), and a Wnt co-receptor, low-density lipoprotein receptor-related protein 6 (LRP6), and inhibited the binding of Wnt3A to Frz8 and LRP6. Although IGF-independent, the cardiogenic effect of IGFBP-4 was attenuated by IGFs through IGFBP-4 sequestration. IGFBP-4 is therefore an inhibitor of the canonical Wnt signalling required for cardiogenesis and provides a molecular link between IGF signalling and Wnt signalling.

The heart is the first organ to form during embryogenesis, and abnormalities in this process result in congenital heart diseases, the most common cause of birth defects in humans[3]. Molecules that mediate cardiogenesis are of particular interest because of their potential use for cardiac regeneration[4,5]. Previous studies have shown that soluble growth factors such as bone morphogenetic proteins (BMPs), fibroblast growth factors (FGFs), Wnts and Wnt inhibitors mediate the tissue interactions that are crucial for cardiomyocyte specification[3,4]. We proposed that there might be additional soluble factors that modulate cardiac development and/or cardiomyocyte differentiation.

P19CL6 cells differentiate into cardiomyocytes with high efficiency in the presence of 1% dimethylsulphoxide (DMSO)[6]. We cultured P19CL6 cells with culture media conditioned by various cell types in the absence of DMSO, and screened the cardiogenic activity of the conditioned media. The extent of cardiomyocyte differentiation was assessed by the immunostaining with MF20 monoclonal antibody that recognizes sarcomeric myosin heavy chain (MHC). Among the several cell types tested, culture media conditioned by a murine stromal cell line OP9 induced cardiomyocyte differentiation of P19CL6 cells without DMSO treatment (Fig. 1a, left and middle panels). Increased MF20-positive area was accompanied by the induction of cardiac marker genes such as *αMHC*, *Nkx2.5* and *GATA-4*, and by the increased protein levels of cardiac troponin T (cTnT) (Fig. 1a, right panel). In contrast, culture media conditioned by COS7 cells, mouse embryonic fibroblasts, NIH3T3 cells, HeLa cells, END2 cells (visceral endoderm-like cells), neonatal rat cardiomyocytes and neonatal rat cardiac fibroblasts did not induce cardiomyocyte differentiation of P19CL6 cells in the absence of DMSO (Fig. 1a and data not shown). From these observations, we postulated that OP9 cells secrete one or more cardiogenic growth factors.

To identify an OP9-derived cardiogenic factor, complementary DNA clones isolated by a signal sequence trap method from an OP9 cell cDNA library[7] were tested for their cardiogenic activities by transient transfection. When available, recombinant proteins were also used to confirm the results. Among candidate factors tested, IGFBP-4 induced cardiomyocyte differentiation of P19CL6 cells, as demonstrated by the increase in MF20-positive area and the induction of cardiac markers (Fig. 1b). We also cultured P19CL6 cells with OP9-conditioned media pretreated with an anti-IGFBP-4 neutralizing antibody. The application of an anti-IGFBP-4 neutralizing antibody attenuated the efficiency of cardiomyocyte differentiation induced by OP9-conditioned media (Fig. 1c). These findings strongly suggest that IGFBP-4 is a cardiogenic factor secreted from OP9 cells.

Because IGFBPs have been characterized as molecules that bind to and modulate the actions of IGFs, we tested whether IGFBP-4 promotes cardiogenesis by either enhancing or inhibiting the actions of IGFs. We first treated P19CL6 cells with a combination of anti-IGF-I and IGF-II-neutralizing antibodies or a neutralizing antibody against type-I IGF receptor. If IGFBP-4 induces cardiomyocyte differentiation by inhibiting IGF signalling, treatment with these antibodies should induce cardiomyocyte differentiation and/or enhance the cardiogenic effects of IGFBP-4. In contrast, if IGFBP-4 promotes cardiogenesis by enhancing IGF signalling, treatment with these antibodies should attenuate IGFBP-4-mediated cardiogenesis. However, treatment with these antibodies did not affect the efficiency of IGFBP-4-induced cardiomyocyte differentiation (Fig. 1d and data not shown). Treatment of P19CL6 cells with IGF-I and IGF-II also did not induce cardiomyocyte differentiation (data not shown). Furthermore, treatment with an IGFBP-4 mutant (IGFBP-4-H74P; His 74 replaced by Pro)[8] that is unable to bind IGFs induced cardiomyocyte differentiation of P19CL6 cells even more efficiently than wild-type IGFBP-4 (Fig. 1e). This is presumably due to the sequestration of wild-type IGFBP-4 but not mutant IGFBP-4-H74P by endogenous IGFs. In agreement with this idea, exogenous IGFs attenuated wild-type IGFBP-4-induced but not IGFBP-4-H74P-induced cardiogenesis (Fig. 1f). Taken together, these observations indicate

[1]Department of Cardiovascular Science and Medicine, Chiba University Graduate School of Medicine, Chiba 260-8670, Japan. [2]ICORP Organ Regeneration Project, Japan Science and Technology Agency (JST), Tokyo 153-8902, Japan. [3]Institute of Stem Cell Biology and Regenerative Medicine, Stanford University School of Medicine, Stanford, California 94305, USA. [4]Department of Reproductive Biology, National Institute for Child Health and Development, Tokyo 157-8535, Japan. [5]Department of Biochemistry, Graduate School of Biomedical Sciences, Hiroshima University, Hiroshima 734-8551, Japan. [6]Department of Life Sciences (Biology), Graduate School of Arts and Science, The University of Tokyo, Tokyo 153-8902, Japan. [7]National Institute of Advanced Industrial Sciences and Technology (AIST), Ibaraki 305-8562, Japan.
*These authors contributed equally to this work.

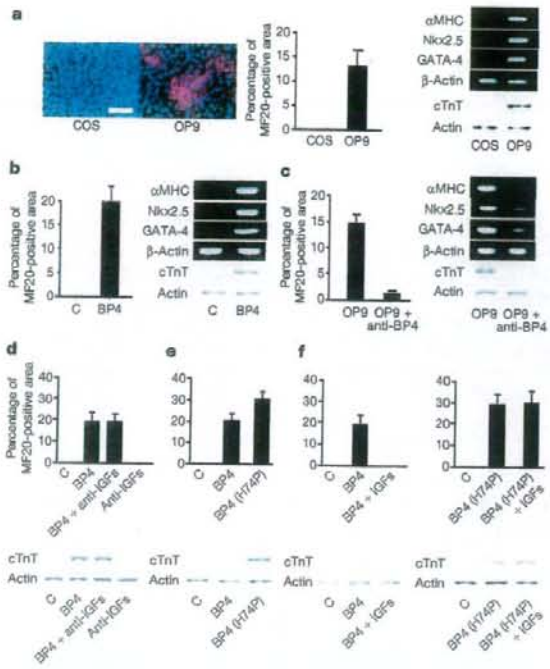

Figure 1 | IGFBP-4 promotes cardiomyocyte differentiation in an IGF-independent manner. a, Culture media conditioned by OP9 cells but not by COS7 cells induced cardiomyocyte differentiation of P19CL6 cells as assessed by MF20-positive area, cardiac marker-gene expression and cTnT protein expression. Scale bar, 100 μm. Error bars show s.d. **b**, Treatment with IGFBP-4 (1 μg ml^{-1}) induced cardiomyocyte differentiation of P19CL6 cells in the absence of DMSO. Error bars show s.d. **c**, Treatment with a neutralizing antibody against IGFBP-4 (anti-BP4; 40 μg ml^{-1}) attenuated cardiomyocyte differentiation of P19CL6 cells induced by OP9-conditioned media. Error bars show s.d. **d**, Treatment with neutralizing antibodies against IGF-I and IGF-II (anti-IGFs; 5 μg ml^{-1} each) had no effect on IGFBP-4-induced cardiomyocyte differentiation of P19CL6 cells. Error bars show s.d. **e**, Mutant IGFBP-4 (BP4(H74P)) that is incapable of binding to IGFs retained cardiomyogenic activity. Error bars show s.d. **f**, IGFs (100 ng ml^{-1} each) attenuated wild-type IGFBP-4-induced but not mutant IGFBP-4-H74P-induced cardiomyocyte differentiation of P19CL6 cells. Error bars show s.d.

that IGFBP-4 induces cardiomyocyte differentiation in an IGF-independent fashion.

To explore further the mechanisms by which IGFBP-4 induces cardiomyogenesis, we tested the hypothesis that IGFBP-4 might modulate the signals activated by other secreted factors implicated in cardiogenesis. It has been shown that canonical Wnt signalling is crucial in cardiomyocyte differentiation[3,4]. In P19CL6 cells, Wnt3A treatment activated β-catenin-dependent transcription of the TOPFLASH reporter gene, and this activation was attenuated by IGFBP-4 (Fig. 2a). Wnt/β-catenin signalling is transduced by the cell-surface receptor complex consisting of Frizzled and low-density-lipoprotein receptor (LDLR)-related protein 5/6 (LRP5/6)[9] and IGFBP-4 attenuated TOPFLASH activity enhanced by the expression of LRP6 or Frizzled 8 (Frz8) (Fig. 2a). As a control, IGFBP-4 did not alter BMP-mediated activation of a BMP-responsive reporter BRE–luc (Supplementary Fig. 1b). These findings suggest that IGFBP-4 is a specific inhibitor of the canonical Wnt pathway. To examine this possibility *in vivo*, we performed axis duplication assays in *Xenopus* embryos. Injection of *Xwnt8* or *Lrp6* mRNA caused secondary axis formation, and injection of *Xenopus IGFBP-4* (*XIGFBP-4*) mRNA alone had minimal effects on axis formation. However, Xwnt8-induced or LRP6-induced secondary axis formation was efficiently blocked by coexpression of XIGFBP-4 (Fig. 2b, c), indicating that IGFBP-4 inhibits canonical Wnt signalling *in vivo*. To explore the mechanisms of Wnt inhibition by IGFBP-4, *Xenopus* animal cap assays and TOPFLASH reporter gene assays were performed. In animal cap assays, IGFBP-4 inhibited LRP6-induced but not β-catenin-induced Wnt-target gene expression (Supplementary Fig. 1c). Similarly, IGFBP-4 attenuated Wnt3A-induced or LRP6-induced TOPFLASH activity but did not alter Dishevelled-1 (Dvl-1)-induced, LiCl-induced or β-catenin-induced TOPFLASH activity (Supplementary Fig. 1d, e). These findings suggest that IGFBP-4 inhibits canonical Wnt signalling at the level of cell-surface receptors. To examine whether IGFBP-4 antagonizes Wnt signalling via direct physical interaction with LRP5/6 or Frizzled, we produced conditioned media containing the Myc-tagged extracellular portion of LRP6 (LRP6N–Myc), the Myc-tagged cysteine-rich domain (CRD) of Frz8 (Frz8CRD–Myc), and V5-tagged IGFBP-4 (IGFBP-4–V5). Immunoprecipitation (IP)/western blot experiments revealed that IGFBP-4 interacted with LRP6N (Fig. 2d) and Frz8CRD (Fig. 2e). A liquid-phase binding assay with ^{125}I-labelled IGFBP-4 and conditioned media containing LRP6N–Myc or Frz8CRD–Myc demonstrated that the interaction between IGFBP-4 and LRP6N or Frz8CRD was specific and saturable (Fig. 2f, g). A Scatchard plot analysis revealed two binding sites with different binding affinities for LRP6N (Fig. 2f, inset) and a single binding site for Frz8CRD (Fig. 2g, inset). A similar binding assay with ^{125}I-labelled Wnt3A demonstrated that IGFBP-4 inhibited Wnt3A binding to LRP6N (Fig. 2h) and Frz8CRD (Fig. 2i), and a Lineweaver–Burk plot revealed that IGFBP-4 was a competitive inhibitor of the binding of Wnt3A to Frz8CDR (Supplementary Fig. 2a). IP/western blot analyses with various deletion mutants of LRP6 and IGFBP-4 revealed that IGFBP-4 interacted with multiple domains of LRP6 and that the carboxy-terminal thyroglobulin domain of IGFBP-4 was required for IGFBP-4 binding to LRP6 or Frz8CRD (Supplementary Fig. 2b–f). It has been shown that inhibition of canonical Wnt signalling promotes cardiomyocyte differentiation in embryonic stem (ES) cells and in chick, *Xenopus* and zebrafish embryos[4,10,11]. These results therefore collectively suggest that IGFBP-4 promotes cardiogenesis by antagonizing the Wnt/β-catenin pathway through direct interactions with Frizzled and LRP5/6.

Next we investigated the role of endogenous IGFBP-4 in P19CL6 cell differentiation into cardiomyocytes. Reverse transcriptase-mediated polymerase chain reaction (RT–PCR) analysis revealed that the expression of *Igfbp4* was upregulated during DMSO-induced P19CL6 cell differentiation (Fig. 3a). Expression of *Igfbp3* and *Igfbp5* was also upregulated in the early and the late phases of differentiation, respectively. Expression of *Igfbp2* was not altered, and that of *Igfbp1* or *Igfbp6* was not detected. When IGFBP-4 was knocked down by two different small interfering RNA (siRNA) constructs, DMSO-induced cardiomyocyte differentiation was inhibited in both cases (Fig. 3b). In contrast, knockdown of *Igfbp3* or *Igfbp5* did not inhibit DMSO-induced cardiomyocyte differentiation (Fig. 3b, right panel). Treatment with an anti-IGFBP-4 neutralizing antibody also blocked DMSO-induced cardiomyocyte differentiation (Fig. 3c). Secretion of endogenous IGFBP-4 is therefore required for the differentiation of P19CL6 cells into cardiomyocytes. Immunostaining for IGFBP-4 revealed that cardiac myocytes were surrounded by the IGFBP-4-positive cells, suggesting that a paracrine effect of IGFBP-4 on cardiomyocyte differentiation is predominant (Fig. 3d). Essentially the same results were obtained in ES cells (Supplementary Fig. 3d–g). To investigate whether IGFBP-4 promotes the differentiation of P19CL6 cells into cardiomyocytes by the inhibition of the canonical Wnt pathway, we expressed dominant-negative LRP6 (LRP6N) in P19CL6 cells. Expression of LRP6N enhanced cardiomyocyte differentiation of P19CL6 cells and reversed the inhibitory effect of *Igfbp4*

knockdown on cardiomyogenesis (Fig. 3e). These observations suggest that endogenous IGFBP-4 is required for cardiomyocyte differentiation of P19CL6 cells and ES cells, and that the cardiogenic effect of IGFBP-4 is mediated by its inhibitory effect on Wnt/β-catenin signalling.

The role of endogenous IGFBP-4 in cardiac development *in vivo* was also examined with *Xenopus* embryos. Whole-mount *in situ* hybridization analysis revealed that strong expression of *XIGFBP-4* was detected at stage 38 in the anterior part of the liver adjacent to the heart (Fig. 4a). Knockdown of *XIGFBP-4* by two different morpholino (MO) constructs resulted in cardiac defects, with more than 70% of the embryos having a small heart or no heart (Fig. 4b). The specificity of MO was confirmed by the observation that simultaneous injection of MO-resistant *XIGFBP-4* cDNA rescued the MO-induced cardiac defects (Fig. 4b, Supplementary Fig. 4c). Coexpression of IGF-binding-defective XIGFBP-4 mutant (XIGFBP-4-H74P) or dominant-negative LRP6 (LRP6N) also rescued the cardiac defects induced by *XIGFBP-4* knockdown (Fig. 4b), whereas overexpression of Xwnt8 in the heart-forming region resulted in cardiac defects similar to those induced by *XIGFBP-4* knockdown (Supplementary Fig. 4d–f), supporting the notion that the cardiogenic effect of IGFBP-4 is independent of IGFs but is mediated by inhibition of the Wnt/β-catenin pathway. The temporal profile of cardiac defects induced by *XIGFBP-4* knockdown was also examined by *in situ* hybridization with *cardiac troponin I* (*cTnI*) (Fig. 4c). At stage 34, morphology of the heart was comparable between control embryos and MO-injected embryos. However, at stage 38, when *XIGFBP-4* starts to be expressed in the anterior part of the liver, the expression of *cTnI* was markedly attenuated in MO-injected embryos; expression of *cTnI* was diminished and no heart-like structure was observed at stage 42. Thus, the heart is initially formed but its subsequent growth is perturbed in the absence of XIGFBP-4, suggesting that IGFBP-4

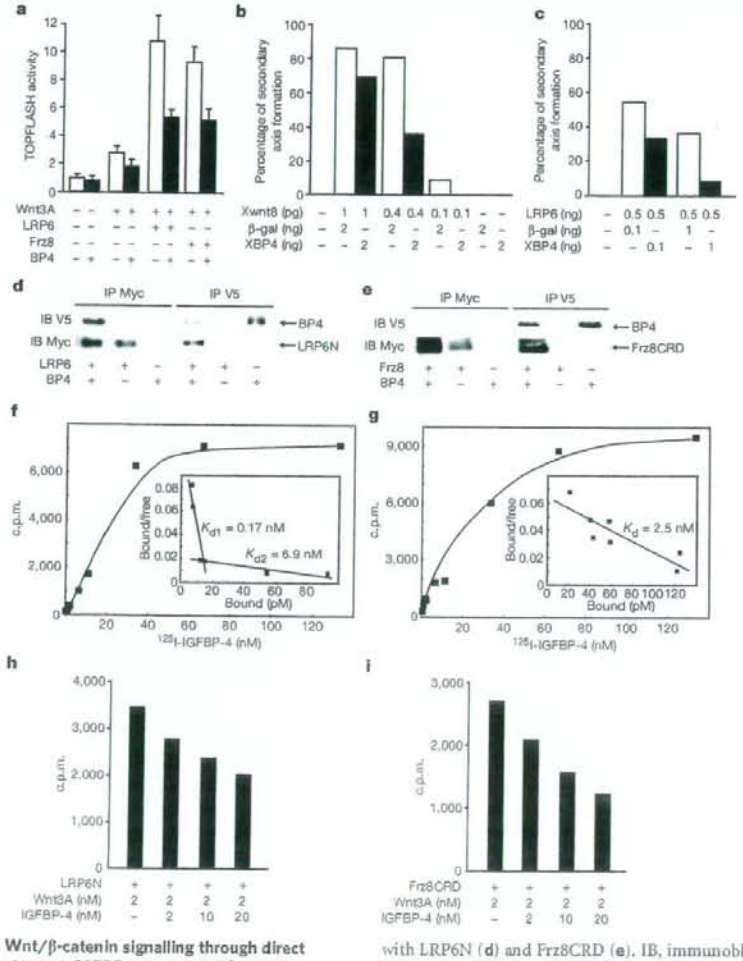

Figure 2 | IGFBP-4 inhibits Wnt/β-catenin signalling through direct interactions with Wnt receptors. a, IGFBP-4 attenuated β-catenin-dependent transcription in P19CL6 cells. P19CL6 cells were transfected with TOPFLASH reporter gene and expression vectors for LRP6 or Frz8, and then treated with Wnt3A or Wnt3A plus IGFBP-4; luciferase activities were then measured. Error bars show s.d. **b**, XIGFBP-4 (XBP4) inhibited Xwnt8-induced secondary-axis formation in *Xenopus* embryos ($n = 20$ for each group). **c**, IGFBP-4 inhibited LRP6-induced secondary-axis formation in *Xenopus* embryos ($n = 30$ for each group). **d**, **e**, IGFBP-4 interacted directly with LRP6N (**d**) and Frz8CRD (**e**). IB, immunoblotting; IP, immunoprecipitation. **f**, A binding assay between ^{125}I-labelled IGFBP-4 and LRP6N. The inset is a Scatchard plot showing two binding sites with different binding affinities. **g**, A binding assay between ^{125}I-labelled IGFBP-4 and Frz8CRD. The inset is a Scatchard plot showing a single binding site. **h**, **i**, IGFBP-4 inhibited Wnt3A binding to LRP6N (**h**) or Frz8CRD (**i**). ^{125}I-labelled Wnt3A binding to LRP6N or Frz8CRD was assessed in the presence of increasing amounts of IGFBP-4.

promotes cardiogenesis by maintaining the proliferation and/or survival of embryonic cardiomyocytes.

It has been shown that canonical Wnt signals inhibit cardiogenesis in chick and frog embryos, and that Wnt antagonists such as Dkk1 and Crescent secreted from the anterior endoderm or the organizer region counteract the Wnt-mediated inhibitory signals and induce cardiogenesis in the anterior lateral mesoderm[4]. However, IGFBP-4-mediated Wnt inhibition is required at later stages of development, when the heart is already formed at the ventral portion and starts to grow and remodel to maintain embryonic circulation. It has been shown that Wnt/β-catenin signalling has time-dependent effects on cardiogenesis in ES cells: canonical Wnt signalling in the early phase of ES-cell differentiation promotes cardiomyogenesis, whereas it inhibits cardiomyocyte differentiation in the late phase[10–12]. In agreement with this notion, IGFBP-4 promoted cardiomyocyte differentiation of ES cells only when IGFBP-4 was applied in the late phase after embryoid body formation (Supplementary Fig. 3a–c). Similar time-dependent effects of Wnt/β-catenin signalling on cardiogenesis has been shown in zebrafish embryos[11]. Moreover, several recent reports suggest that Wnt/β-catenin signalling is a positive regulator of cardiac progenitor-cell proliferation in the secondary heart field[13]. It therefore seems that canonical Wnt signalling has divergent effects on cardiogenesis at multiple stages of development: first, canonical Wnt signalling promotes cardiogenesis at the time of gastrulation or mesoderm specification; second, it inhibits cardiogenesis at the time when cardiac mesoderm is specified in the anterior lateral mesoderm; third, it promotes the expansion of cardiac progenitors in the secondary heart field; and fourth, it inhibits cardiogenesis at later stages when the embryonic heart is growing. It is interesting to note that IGFBP-4 is expressed predominantly in the liver. Mouse IGFBP-4 is

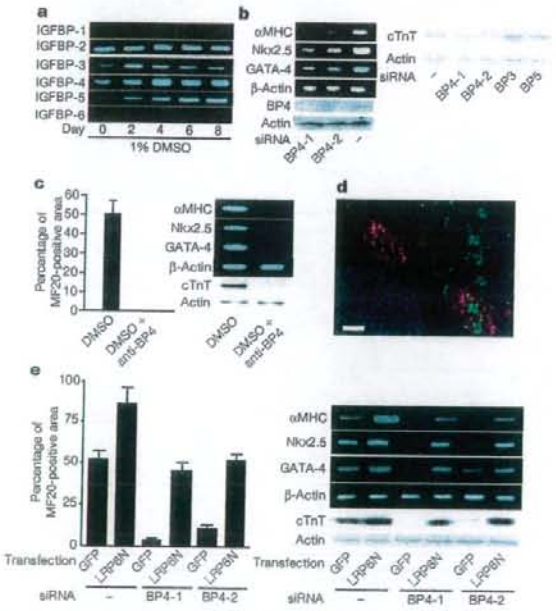

Figure 3 | IGFBP-4 is required for the differentiation of P19CL6 cells into cardiomyocytes. **a**, Expression analysis of IGFBP family members by RT–PCR during DMSO-induced cardiomyocyte differentiation of P19CL6 cells (from day 0 to day 8). **b**, Left: knockdown of *Igfbp4* in P19CL6 cells attenuated cardiac marker expression in response to treatment with DMSO. BP4-1 and BP4-2 represent two different siRNAs for IGFBP-4. Right: knockdown of *Igfbp3* or *Igfbp5* had no effect on cTnT expression in response to DMSO treatment. **c**, Treatment with a neutralizing antibody against IGFBP-4 (anti-BP4; 40 μg ml^{-1}) attenuated DMSO-induced cardiomyocyte differentiation of P19CL6 cells. Error bars show s.d. **d**, IGFBP-4 immunostaining during DMSO-induced differentiation of P19CL6 cells stably transfected with αMHC–green fluorescent protein (GFP) reporter gene. Top left, IGFBP-4 staining (red); top right, GFP expression representing differentiated cardiomyocytes; bottom left, nuclear staining with DAPI (4′,6-diamidino-2-phenylindole); bottom right, a merged picture. Scale bar, 100 μm. **e**, Attenuated cardiomyocyte differentiation of P19CL6 cells by *Igfbp4* knockdown was rescued by inhibiting Wnt/β-catenin signalling. Control and *Igfbp4*-knocked-down P19CL6 cells were transfected with an expression vector for GFP or LRP6N (a dominant-negative form of LRP6) and induced to differentiate into cardiomyocytes by treatment with DMSO. LRP6N overexpression rescued the attenuated cardiomyocyte differentiation induced by *Igfbp4* knockdown as assessed by MF20-positive area (left panel), cardiac marker-gene expression and cTnT protein expression (right panel). Error bars show s.d.

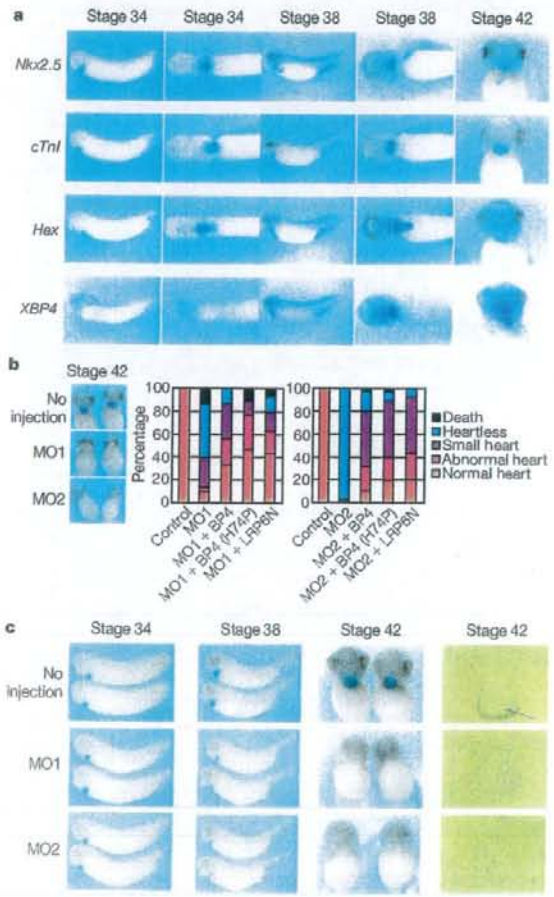

Figure 4 | IGFBP-4 is required for the maturation of the heart in *Xenopus* embryos. **a**, *In situ* hybridization analysis of *Nkx2.5* (an early cardiac marker), *cTnI* (a mature cardiac marker), *Hex* (a liver marker), and *XIGFBP-4* (*XBP4*) mRNA expression at stages 34, 38 and 42. **b**, Knockdown of *XIGFBP-4* by two different morpholinos (MO1 and MO2) resulted in severe cardiac defects as assessed by *cTnI in situ* hybridization at stage 42 (left). These cardiac defects were rescued by simultaneous injection of MO-resistant wild-type XIGFBP-4, mutant XIGFBP-4-H74P (BP4(H74P)) and LRP6N ($n = 30$ for each group). **c**, Temporal profile of cardiac defects induced by *XIGFBP-4* knockdown. Morphology of the heart as assessed by *cTnI in situ* hybridization was almost normal at stage 34 but was severely perturbed at stages 38 and 42. The right column shows sections of control and MO-injected embryos. The arrow indicates the heart in control embryos. No heart-like structure was observed in MO-injected embryos.

also strongly expressed in the tissues adjacent to the heart such as pharyngeal arches and liver bud at embryonic day (E)9.5 (Supplementary Fig. 3h). These observations and the results of IGFBP-4 immunostaining in P19CL6 cells and ES cells suggest that IGFBP-4 promotes cardiogenesis in a paracrine fashion. Together with a previous report showing that cardiac mesoderm secretes FGFs and induces liver progenitors in the ventral endoderm[14], these observations suggest that there exist reciprocal paracrine signals between the heart and the liver that coordinately promote the development of each other.

IGFBPs are composed of six members, IGFBP-1 to IGFBP-6. Reporter gene assays and β-catenin stabilization assays revealed that IGFBP-4 was the most potent canonical Wnt inhibitor and that IGFBP-1, IGFBP-2 and IGFBP-6 also showed modest activity in Wnt inhibition, whereas IGFBP-3 and IGFBP-5 had no such activity (Supplementary Fig. 5a–c). In agreement with this, IP/western blot analyses demonstrated that IGFBP-1, IGFBP-2, IGFBP-4 and IGFBP-6 but not IGFBP-3 or IGFBP-5 interacted with LRP6 or Frz8CRD (Supplementary Fig. 5d, e). Thus, the lack of cardiac phenotypes in IGFBP-4-null mice or IGFBP-3/IGFBP-4/IGFBP-5 triple knockout mice[15] may be due to genetic redundancies between IGFBP-4 and other IGFBPs such as IGFBP-1, IGFBP-2 and/or IGFBP-6.

The identification of IGFBP-4 as an inhibitor of Wnt/β-catenin signalling may also have some implications for cancer biology[16]. It was shown that treatment with IGFBP-4 reduces cell proliferation in some cancer cell lines *in vitro*, and that overexpression of IGFBP-4 attenuates the growth of prostate cancer *in vivo*. Decreased serum levels of IGFBP-4 are associated with the risk of breast cancer. Because the activation of Wnt signalling is implicated in several forms of malignant tumours[17,18], it is possible that the inhibitory effect of IGFBP-4 on cell proliferation is mediated in part by the inhibition of canonical Wnt signalling.

METHODS SUMMARY

Cell culture. P19CL6 cells and ES cells were cultured and induced to differentiate into cardiomyocytes essentially as described[6,19]. P19CL6 cells (2,000 cells per 35-mm dish) were treated with various conditioned media for screening of their cardiogenic activities. For siRNA-mediated knockdown, pSIREN-RetroQ vectors (Clontech) ligated with double-stranded oligonucleotides were transfected into P19CL6 cells or ES cells, and puromycin-resistant clones were selected.

IP/western blot analyses and binding assays. Conditioned media for IP/western blot analyses were produced by using 293 cells. Binding reactions were performed overnight at 4 °C. ^{125}I-labelling of IGFBP-4 and Wnt3A was performed with IODO-BEADS Iodination Reagent (Pierce). A liquid-phase binding assay was performed essentially as described[19].

***Xenopus* experiments.** Axis duplication assays, animal cap assays, and *in situ* hybridization analyses in *Xenopus* were performed essentially as described[20]. Electroporation of mRNA was performed at stage 28 essentially as described[21].

Full Methods and any associated references are available in the online version of the paper at www.nature.com/nature.

Received 22 August 2007; accepted 24 April 2008.
Published online 4 June 2008.

1. Firth, S. M. & Baxter, R. C. Cellular actions of the insulin-like growth factor binding proteins. *Endocr. Rev.* 23, 824–854 (2002).
2. Mohan, S. & Baylink, D. J. IGF-binding proteins are multifunctional and act via IGF-dependent and -independent mechanisms. *J. Endocrinol.* 175, 19–31 (2002).
3. Olson, E. N. & Schneider, M. D. Sizing up the heart: development redux in disease. *Genes Dev.* 17, 1937–1956 (2003).
4. Foley, A. & Mercola, M. Heart induction: embryology to cardiomyocyte regeneration. *Trends Cardiovasc. Med.* 14, 121–125 (2004).
5. Leri, A., Kajstura, J. & Anversa, P. Cardiac stem cells and mechanisms of myocardial regeneration. *Physiol. Rev.* 85, 1373–1416 (2005).
6. Monzen, K. *et al.* Bone morphogenetic proteins induce cardiomyocyte differentiation through the mitogen-activated protein kinase kinase kinase TAK1 and cardiac transcription factors Csx/Nkx-2.5 and GATA-4. *Mol. Cell. Biol.* 19, 7096–7105 (1999).
7. Ueno, H. *et al.* A stromal cell-derived membrane protein that supports hematopoietic stem cells. *Nature Immunol.* 4, 457–463 (2003).
8. Qin, X., Strong, D. D., Baylink, D. J. & Mohan, S. Structure–function analysis of the human insulin-like growth factor binding protein-4. *J. Biol. Chem.* 273, 23509–23516 (1998).
9. Moon, R. T., Kohn, A. D., De Ferrari, G. V. & Kaykas, A. WNT and β-catenin signalling: diseases and therapies. *Nature Rev. Genet.* 5, 691–701 (2004).
10. Naito, A. T. *et al.* Developmental stage-specific biphasic roles of Wnt/β-catenin signaling in cardiomyogenesis and hematopoiesis. *Proc. Natl Acad. Sci. USA* 103, 19812–19817 (2006).
11. Ueno, S. *et al.* Biphasic role for Wnt/β-catenin signaling in cardiac specification in zebrafish and embryonic stem cells. *Proc. Natl Acad. Sci. USA* 104, 9685–9690 (2007).
12. Liu, Y. *et al.* Sox17 is essential for the specification of cardiac mesoderm in embryonic stem cells. *Proc. Natl Acad. Sci. USA* 104, 3859–3864 (2007).
13. Cohen, E. D., Tian, Y. & Morrisey, E. E. Wnt signaling: an essential regulator of cardiovascular differentiation, morphogenesis and progenitor self-renewal. *Development* 135, 789–798 (2008).
14. Jung, J., Zheng, M., Goldfarb, M. & Zaret, K. S. Initiation of mammalian liver development from endoderm by fibroblast growth factors. *Science* 284, 1998–2003 (1999).
15. Ning, Y. *et al.* Diminished growth and enhanced glucose metabolism in triple knockout mice containing mutations of insulin-like growth factor binding protein-3, -4, and -5. *Mol. Endocrinol.* 20, 2173–2186 (2006).
16. Durai, R. *et al.* Biology of insulin-like growth factor binding protein-4 and its role in cancer. *Int. J. Oncol.* 28, 1317–1325 (2006).
17. Logan, C. Y. & Nusse, R. The Wnt signaling pathway in development and disease. *Annu. Rev. Cell Dev. Biol.* 20, 781–810 (2004).
18. Clevers, H. Wnt/β-catenin signaling in development and disease. *Cell* 127, 469–480 (2006).
19. Semenov, M. V. *et al.* Head inducer Dickkopf-1 is a ligand for Wnt coreceptor LRP6. *Curr. Biol.* 11, 951–961 (2001).
20. Kobayashi, H. *et al.* Novel Daple-like protein positively regulates both the Wnt/β-catenin pathway and the Wnt/JNK pathway in *Xenopus*. *Mech. Dev.* 122, 1138–1153 (2005).
21. Sasagawa, S., Takabatake, T., Takabatake, Y., Muramatsu, T. & Takeshima, K. Improved mRNA electroporation method for *Xenopus* neurula embryos. *Genesis* 33, 81–85 (2002).

Supplementary Information is linked to the online version of the paper at www.nature.com/nature.

Acknowledgements We thank E. Fujita, R. Kobayashi and Y. Ishiyama for technical support; T. Yamauchi and K. Ueki for advice on binding assays; and Y. Oruma and S. Takahashi for advice on *Xenopus* electroporation. This work was supported by grants from the Ministry of Education, Culture, Sports, Science and Technology (MEXT), the Ministry of Health, Labour, and Welfare, and the New Energy and Industrial Technology Development Organization (NEDO).

Author Contributions W.Z., I.S. and Y.I. contributed equally to this work. I.K. designed and supervised the research. W.Z., I.S., Y.I., Z.L., H.I., M.Y. and A.T.N. performed experiments. J.N., H.U., A.U., T.M., T.N., A.K. and M.A. contributed new reagents and/or analytical tools. W.Z., I.S., Y.I., A.K. and I.K. analysed data. W.Z., I.S., Y.I. and I.K. prepared the manuscript.

Author Information Reprints and permissions information is available at www.nature.com/reprints. Correspondence and requests for materials should be addressed to I.K. (komuro-tky@umin.ac.jp).

METHODS

Plasmids and reagents. cDNA clones encoding mouse IGFBPs and *Xenopus* IGFBP-4 were purchased from Open Biosystems. XIGFBP-4-H74P mutant was generated with a QuickChange Site-Directed Mutagenesis kit (Stratagene). His-tagged human wild-type IGFBP-4 and mutant IGFBP-4-H74P (vectors provided by X. Qin)[8] were produced and purified with HisTrap HP Kit (Amersham). Full-length Frz8, Frz8CRD and LRP6N were provided by X. He[22,23]. Full-length LRP6, membrane-bound forms of LRP6 deletion mutants, and Dkk1 were from C. Niehrs[24]. pXwnt8 and pCSKA-Xwnt8 were from J. Christian[25]. pCS2–β-catenin was from D. Kimelman[26]. αMHC–GFP was from B. Fleischmann[27]. BRE–luc was from P. ten Dijke[28]. pCGN-Dvl-1 was described previously[29]. Soluble forms of LRP6 deletion mutants and probes for *in situ* hybridization analysis (Nkx2.5, cTnI and Hex) were generated by PCR. IGFBP-4, Wnt3A, IGF-I, IGF-II and BMP2 were from R&D. Neutralizing antibodies were from R&D (anti-IGFBP-4), Sigma (anti-IGF-I and anti-IGF-II), and Oncogene (anti-type-I IGF receptor). The antibodies used for immunoprecipitation, western blotting and immunostaining were from Invitrogen (anti-Myc, anti-V5), Santa Cruz (anti-cTnT, anti-IGFBP-4, anti-topoisomerase I (TOPO-I)), Sigma (anti-β-actin, anti-β-catenin, anti-FLAG (M2)) and Developmental Studies Hybridoma Bank (anti-sarcomeric myosin heavy chain (MF20)).

Cell culture experiments. P19CL6 cells and ES cells were cultured and induced to differentiate into cardiomyocytes essentially as described[8,10]. P19CL6 cells (2,000 cells per 35-mm dish) were treated with various conditioned media for screening of their cardiogenic activities. P19CL6 cells or ES cells stably transfected with αMHC promoter driven–GFP were generated by transfection of αMHC–GFP plasmid into P19CL6 cells or ht7 ES cells followed by G418 selection. Luciferase reporter gene assays, western blot analyses, immunostaining and RT–PCR were performed as described[10]. Reporter gene assays were repeated at least three times. PCR primers and PCR conditions are listed in Supplementary Table 1. For siRNA-mediated knockdown, siRNAs were expressed with pSIREN-RetroQ vector (Clontech). Oligonucleotide sequences used are listed in Supplementary Table 2. pSIREN-RetroQ vectors ligated with double-stranded oligonucleotides were transfected into P19CL6 cells or ES cells, and puromycin-resistant clones were isolated and expanded. For β-catenin stabilization assays, nuclear extracts of L cells were prepared with NE-PER Nuclear and Cytoplasmic Extraction Reagents (Pierce). Data are shown as means and s.d.

IP/western blot analyses and binding assays. Conditioned media for IP/western blot analyses containing full-length or various deletion mutants of IGFBPs, LRP6, Frz8CRD and Dkk1 were produced with 293 cells. Binding reactions were performed overnight at 4 °C. Immunoprecipitation was performed with Protein G–Sepharose 4 Fast Flow (Amersham). ^{125}I-labelling of IGFBP-4 and Wnt3A was performed with IODO-BEADS Iodination Reagent (Pierce). A liquid-phase binding assay was performed essentially as described[19]. In brief, conditioned media containing LRP6N–Myc or Frz8CRD–Myc were mixed with various concentrations of ^{125}I-labelled IGFBP-4 and incubated overnight at 4 °C. LRP6N–Myc or Frz8CRD–Myc was immunoprecipitated and the radioactivity of bound IGFBP-4 was measured after extensive washing of the Protein G–Sepharose beads. For a competitive binding assay, conditioned media containing LRP6N–Myc or Frz8CRD–Myc were mixed with ^{125}I-labelled Wnt3A and unlabelled IGFBP-4, and incubated overnight at 4 °C. LRP6N–Myc or Frz8CRD–Myc was then immunoprecipitated and the radioactivity of bound Wnt3A was measured.

***Xenopus* experiments and mouse *in situ* hybridization analysis.** Axis duplication assays, animal cap assays and *in situ* hybridization analyses in *Xenopus* were performed essentially as described[20]. Two independent cDNAs for *XIGFBP-4*, presumably resulting from pseudotetraploid genomes, were identified by 5′ rapid amplification of cDNA ends (Supplementary Fig. 4a). Two different MOs targeting both of these two IGFBP-4 transcripts were designed (Gene Tools) (Supplementary Fig. 4a and Supplementary Table 2). MO-sensitive *XIGFBP-4* cDNA including a 41-base-pair 5′-untranslated region (UTR) was generated by PCR. MO-resistant *XIGFBP-4* cDNA (wild-type and H74P mutant) was generated by introducing five silent mutations in the MO1 target sequence and excluding the 5′-UTR (Supplementary Fig. 4a). To determine the specificity of MOs, MO-sensitive or MO-resistant *XIGFBP-4–myc* mRNA was injected into *Xenopus* embryos with or without MOs, and protein/mRNA expression was analysed. PCR primers and PCR conditions are listed in Supplementary Table 1. MOs and plasmid DNAs were injected at the eight-cell stage into the dorsal region of two dorsal–vegetal blastomeres fated to be heart and liver anlage. Electroporation of mRNA was performed essentially as described[21]. Injection of mRNA (5 ng in 5 nl of solution) into the vicinity of heart anlage and application of electric pulses were performed at stage 28. Whole-mount *in situ* hybridization analysis of murine IGFBP-4 was performed as described[30].

22. He, X. *et al.* A member of the Frizzled protein family mediating axis induction by Wnt-5A. *Science* 275, 1652–1654 (1997).
23. Tamai, K. *et al.* LDL-receptor-related proteins in Wnt signal transduction. *Nature* 407, 530–535 (2000).
24. Mao, B. *et al.* LDL-receptor-related protein 6 is a receptor for Dickkopf proteins. *Nature* 411, 321–325 (2001).
25. Christian, J. L. & Moon, R. T. Interactions between Xwnt-8 and Spemann organizer signaling pathways generate dorsoventral pattern in the embryonic mesoderm of *Xenopus*. *Genes Dev.* 7, 13–28 (1993).
26. Yost, C. *et al.* The axis-inducing activity, stability, and subcellular distribution of β-catenin is regulated in *Xenopus* embryos by glycogen synthase kinase 3. *Genes Dev.* 10, 1443–1454 (1996).
27. Kolossov, E. *et al.* Identification and characterization of embryonic stem cell-derived pacemaker and atrial cardiomyocytes. *FASEB J.* 19, 577–579 (2005).
28. Korchynskyi, O. & ten Dijke, P. Identification and functional characterization of distinct critically important bone morphogenetic protein-specific response elements in the Id1 promoter. *J. Biol. Chem.* 277, 4883–4891 (2002).
29. Kishida, M. *et al.* Synergistic activation of the Wnt signaling pathway by Dvl and casein kinase Iε. *J. Biol. Chem.* 276, 33147–33155 (2001).
30. Hosoda, T. *et al.* A novel myocyte-specific gene Midori promotes the differentiation of P19CL6 cells into cardiomyocytes. *J. Biol. Chem.* 276, 35978–35989 (2001).

RBM Online - Vol 16 No 1. 2008 41-50 Reproductive BioMedicine Online; www.rbmonline.com/Article/3061 on web 13 November

Symposium: Nuclear reprogramming and the control of differentiation in mammalian embryos

Elucidating nuclear reprogramming mechanisms: taking a synergistic approach

Dr Hidenori Akutsu became interested in nuclear reprogramming in mammalian species when he was a research fellow at University of Hawaii under Dr Ryuzo Yanagimachi. This interest endured and motivated him to undertake further research under Dr Minoru Ko at NIA/NIH (embryo genomics) and Dr Kevin Eggan at Harvard University (epigenetic and nuclear reprogramming). While at Harvard University he also became an important part of Dr Douglas Melton's team, deriving human embryonic stem cell lines which were later offered freely to the scientific community to facilitate the efforts of other scientists. His special interests are egg development, epigenetic and nuclear reprogramming and embryonic stem cells.

Dr Hidenori Akutsu

Stephen Sullivan[1,3], Justin K Ichida[1], Akihiro Umezawa[2], Hidenori Akutsu[2]
[1]Stowers Medical Institute and Harvard Stem Cell Institute, Department of Cellular and Molecular Biology, Harvard University, 7 Divinity Avenue, SF457, Cambridge 02138, USA; [2]National Research Institute for Child Health and Development Department of Reproductive Biology and Pathology 2–10–1 Okura, Setagaya, Tokyo 157–8535, Japan
[3]Correspondence: e-mail: sullivan@mcb.harvard.edu.

Abstract

Nuclear reprogramming is the process by which a differentiated somatic nucleus has developmental potential restored to it. It involves heritable changes in gene expression as well as structural and functional changes to chromatin structure. This process is naturally induced immediately after fertilization, but can also be artificially induced by nuclear transfer, cell fusion and also now by viral transduction with four stem cell genes. However, the frequency of successful reprogramming is low in each system. The highest success rates, those using nuclear transfer, are only of the order of 2–5%. This article briefly reviews these three methods and proposes a synergistic approach where conditions that facilitate reprogramming in one system are transposed to the others. This might increase the incidence of successful reprogramming and identify common steps necessary for the reacquisition of developmental potential.

Keywords: *developmental potential, differentiation, embryonic stem cell, nuclear reprogramming, nuclear transfer, pluripotency*

Cell differentiation and nuclear reprogramming

Cell differentiation is the process by which a cell becomes specialised to perform specific biological functions (Gurdon, 1968). The process is associated with a decline in the range of cell types that the cell is capable of generating (Gurdon, 1968). It had been initially thought that as cells differentiated, hereditary material no longer required was cast off or permanently inactivated (Weismann, 1893). However, this paradigm was shown to be false more than 50 years ago when Briggs and King transferred differentiated nuclei from blastula cells to enucleated eggs of the frog *Rana pipiens* (Briggs and King, 1952). These reconstructed cells went on to generate normal hatched embryos, showing that nuclei of differentiated cells contain the same genetic material as those of undifferentiated cells. The current paradigm for how cell differentiation occurs involves the assembly of condensed chromosomal structures (Kass and Wolffe, 1998). Such structures, formed via interactions between DNA and protein, are thought to compartmentalize chromatin into functional domains and, in some unknown way, stably maintain the differentiated state even when the cell divides.

In terms of mammalian development, differentiation first occurs at the blastocyst stage in the preimplantation embryo. As the embryo develops, the outer layer cells of the embryo (the trophectoderm) become morphologically distinct from the inner cell mass (ICM). Cells of the trophectoderm and ICM have different developmental potentials, e.g. cells of the ICM have the potential to form all the cells of the conceptus, whereas the trophectoderm cells have only the potential to form extraembryonic cells or the placenta.